Webb, Kevin F. (2014) Condenser-free contrast methods for transmitted-light microscopy. Journal of Microscopy, 257 (1). pp. 8-22. ISSN 0022-2720

Journal of
Microscopy

Journal of Microscopy, Vol. 257, Issue 1 2015, pp. 8–22
Received 27 July 2013; accepted 14 August 2014

doi: 10.1111/jmi.12181

Condenser-free contrast methods for transmitted-light microscopy

K.F. WEBB
Royal Academy of Engineering Research Fellow, Institute of Biophysics, Imaging & Optical Science (IBIOS), School of Electrical and Electronic Engineering, The University of Nottingham, University Park, Nottingham, U.K.

Key words. Condenser-free contrast enhancement, darkfield microscopy, LED illumination, Rheinberg illumination, scanning probe microscopy, Zernike phase contrast microscopy.

Summary

Phase contrast microscopy allows the study of highly transparent yet detail-rich specimens by producing intensity contrast from phase objects within the sample. Presented here is a generalized phase contrast illumination schema in which condenser optics are entirely abrogated, yielding a condenser-free yet highly effective method of obtaining phase contrast in transmitted-light microscopy. A ring of light emitting diodes (LEDs) is positioned within the light-path such that observation of the objective back focal plane places the illuminating ring in appropriate conjunction with the phase ring. It is demonstrated that true Zernike phase contrast is obtained, whose geometry can be flexibly manipulated to provide an arbitrary working distance between illuminator and sample. Condenser-free phase contrast is demonstrated across a range of magnifications (4–100×), numerical apertures (0.13–1.65NA) and conventional phase positions. Also demonstrated is condenser-free darkfield microscopy as well as combinatorial contrast including Rheinberg illumination and simultaneous, colour-contrasted, brightfield, darkfield and Zernike phase contrast. By providing enhanced and arbitrary working space above the preparation, a range of concurrent imaging and electrophysiological techniques will be technically facilitated. Condenser-free phase contrast is demonstrated in conjunction with scanning ion conductance microscopy (SICM), using a notched ring to admit the scanned probe. The compact, versatile LED illumination schema will further lend itself to novel next-generation transmitted-light microscopy designs. The condenser-free illumination method, using rings of independent or radially-scanned emitters, may be exploited in future in other electromagnetic wavebands, including X-rays or the infrared.

Correspondence to: Kevin F. Webb, Ph.D., Royal Academy of Engineering Research Fellow, Institute of Biophysics, Imaging & Optical Science (IBIOS), School of Electrical and Electronic Engineering, The University of Nottingham, University Park, Nottingham NG72RD, U.K. Tel: 0115 951 3233; fax: 0115 846 6580; e-mail: kevin.webb@nottingham.ac.uk

Introduction

Phase contrast microscopy is a ubiquitous imaging technique in the biological sciences, providing a cheap and effective solution for the visualization of transparent samples such as living cells. The basic principle is as follows: illuminating light from an extended source is collimated and an annulus of illumination is selected by inserting a ring-shaped mask into the aperture plane of the condenser assembly (Fig. 1 A). This illuminating annulus is focussed through the sample by the condenser lens as a hollow cone and, in interacting with the sample, is split into two partially coherent beams. The system is aligned such that direct-path light (*solid lines*) impinges on the 'phase ring' located in the back focal plane (BFP) of the phase contrast objective. The natural phase shift of unstained biological specimens is only circa 90° ($\lambda/4$). In standard ('positive') phase contrast, the phase ring is made optically thinner than the rest such that direct light is phase advanced at the image plane by $\lambda/2$ relative to light diffracted by the sample (*dashed* lines), most of which misses the phase ring (Zernike, 1942b). Interference between the two beams produces constructive and destructive interference which creates intensity contrast at the image plane from minute differences in optical path within the sample (Zernike, 1942a).

The fundamental design of commercial phase contrast microscopes has remained largely unaltered since Frits Zernike was awarded the 1953 Nobel prize in Physics for its discovery (Zernike, 1953). Modern variants have been directed against minimizing the characteristic phase 'halo' and 'shade off' artefacts, which are a consequence of a restricted range of illumination angles, diffraction via restricted apertures and the impingement of a portion of the sample-diffracted light onto the phase ring (Zernike, 1942b). Apodised phase objectives (Otaki, 2000) employ a stepped 'apodised' phase ring to 'roll off' halo artefacts by minimizing discontinuities in the aperture plane. A more advanced schema was recently demonstrated (Maurer *et al.*, 2008) using a pair of spatial light modulators to provide a random array of light sources and complementary phase-plates, thus producing phase contrast using the full numerical aperture (NA) of the optical system, while minimizing

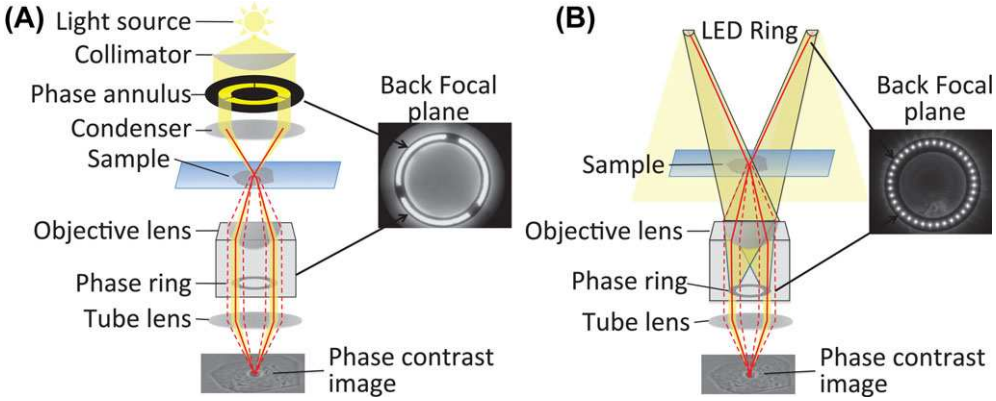

Fig. 1. (A) Optical schema for conventional Zernike phase contrast microscopy, consisting of collimated light source, phase annulus, condenser assembly and phase contrast objective lens. *Inset* view of objective BFP via Bertrand lens showing overlapped phase annulus and phase ring. (B) Optical schema for condenser-free Zernike phase contrast consisting of LED ring and phase contrast objective. *Inset* view of objective BFP showing overlapped image of LED ring and phase ring.

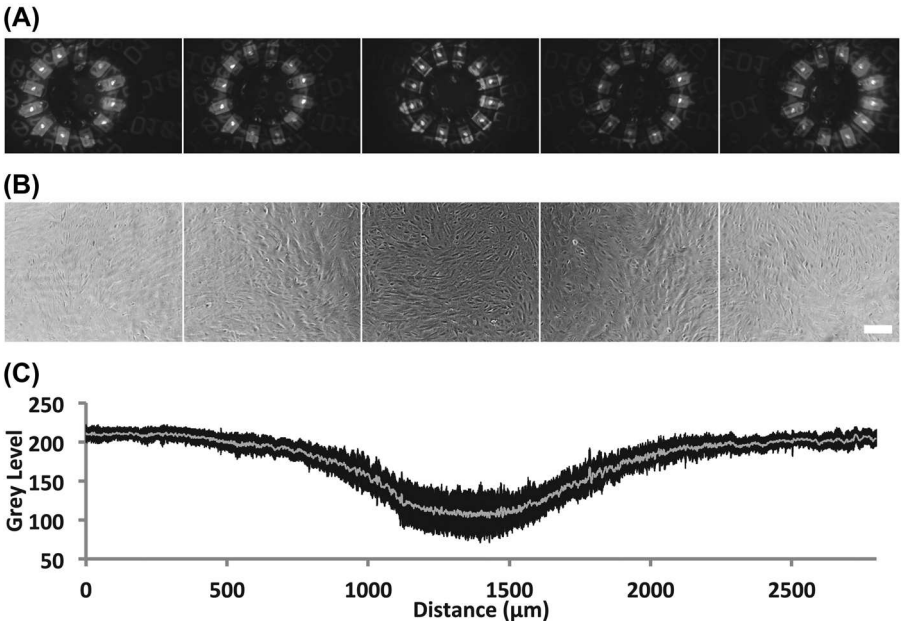

Fig. 2. Analysis of condenser-free phase contrast with *XY* alignment. (A–E) View of 10× 0.3NA Ph1 objective BFP, showing progressive misalignment of LED ring (Ø14 mm, 62 mm above sample) with respect to the phase ring. (F–J) Corresponding phase contrast images of a confluent layer of ARPE-19 cells viewed under alignment conditions in *(A)–(E)*. Scale bar 200 μm. Optimal overlap of LEDs with phase ring *C* produces optimal phase contrast *H*. (K) Each vertical column of pixels in an extended tile of phase contrast images discretised in *F–J* is plotted as mean ± SD to show global drop in intensity and increase in contrast as LED ring is aligned optimally with the phase ring.

cross-talk between sample-diffracted light with the randomly placed 'phase plates' to eliminate halo. Some modern commercial systems also offer an 'external' phase ring option in a conjugate aperture plane, allowing phase contrast to be obtained with nonphase objectives and preserving the full objective aperture for epifluorescence or total internal reflection fluorescence (TIRF) imaging.

Live cells are typically examined using an inverted microscope, where access to the preparation tends to be restricted by the condenser assembly. Commercial condensers for phase contrast range from the simple single-lens-plus-annulus design in simple cell-inspection microscopes through to complex high-NA condensers for high-resolution imaging. A selection of annuli are required to match a range of phase geometries, necessitating a bulky turret, as well as provision for adjustments to centration and focus. The pancratic (Carl Zeiss AG, Jena, Germany) and Heine (Ernst Leitz Optische Werke, Wetzlar, Germany) condensers were developed in the mid-20th

century to provide continuously variable annuli of illumination to satisfy phase and darkfield across a range of objectives by providing what was termed 'circular oblique illumination', employing specialized moving reflecting optics within elaborate and rather costly condenser assemblies.

Restricted access to the cells is a barrier to quality imaging in experiments involving microelectrodes or scanned probes, including patch clamping and scanning ion conductance microscopy (SICM). Kempson reported in the 1950s that a condenser was not strictly necessary for phase contrast microscopy at very low magnifications, using a large diffusing incandescent bulb along with a simple mask (Kempson, 1950). However removal of the condenser to fit SICM or other scanning-probe systems, as is commonly necessary, has disastrous consequences for brightfield imaging. Condenserless phase contrast has been reported in the literature, in parallel with atomic force microscopy (Lugmaier *et al.*, 2005), using a ring of light emitting diodes (LEDs) to produce phase contrast around an obstructing AFM cantilever in a single fixed geometry, using one particular objective lens in a bespoke hybrid instrument.

The current work significantly extends and characterizes condenser-free contrast enhancement into a generally applicable approach which can be adapted, in principle, to any microscope setup. This paper presents, characterizes, and generalizes a condenser-free illumination schema which produces high-quality Zernike phase contrast and darkfield contrast using rings of LEDs; an image of which is projected into the objective BFP using simple lens optics. The approach differs from previous work in that it is shown to possess great geometrical flexibility, and is thereby generally applicable across a wide range of objectives including those of very high magnification and NA. In addition, the linear geometric relationship between sample distance and ring diameter permits the free design of optical systems to match arbitrary phase contrast geometries. The ability to arbitrarily choose the working distance of the condenserless illuminator, which may be varied from a few millimetres to arbitrarily greater distances as appropriate to the experiment. This permits the free introduction of electrodes, fibres, perfusion assemblies, etc. into the preparation without being limited by the condenser assembly.

As well as phase contrast, this paper exploits the geometric flexibility of the condenser-free LED-based illumination system to demonstrate condenser-free darkfield contrast, which conventionally requires condenser assemblies of very high NA, often mirror-based, in order to supply illuminating rays at higher incident angle than the objective can accept. Using this condenser-free schema, darkfield imaging can be arbitrarily applied either in combination or sequentially with both transmitted-light brightfield or phase contrast microscopy to yield additional contrast methods, including Rheinberg illumination (Rheinberg, 1896). The same simple, condenser-free, ring-based design is also capable of producing arbitrarily variable, sequential or simultaneous combinations of brightfield, darkfield and phase contrast microscopy. The use of several discrete LED rings can provide the diverse range of intermediate regimes allowed by the Heine condenser, as well as the combinatorial embodiment described more recently using elaborate bespoke optics (Piper & Piper, 2012a, 2012b, 2012c, 2013a, 2013b).

Materials and methods

Cells

Fresh buccal epithelial strews were prepared by lightly abrading the cheek with a cotton bud and mounting the dislodged cells, immersed in a little saliva, between two coverslips. ARPE-19 (human-derived retinal pigment epithelium), 3T3 (mouse fibroblast) and TE671 (human rhabdomyosarcoma) cultured cell lines were plated on poly-*L*-lysine-coated glass-bottomed Petri dishes in DMEM/HAMS F12 supplemented with 2.5 mML^{-1} glutamine, 10% foetal bovine serum, 100 UmL^{-1} penicillin and 100 $ugmL^{-1}$ streptomycin. Cells were cultured for either 24 h (for individual cells) or 72 h (for confluent cells). For scanning probe imaging, cells were fixed in 4% paraformaldehyde (5 min) and imaged in filtered phosphate-buffered saline, which was also added to the scanned nanoelectrode. For DNA staining, 1:1000 Hoechst stain stock (Sigma-Aldrich, UK) was added to the bath and imaged using Hg lamp illumination (Ex:355/25, Em:420LP).

Microscope

A Nikon Ti Eclipse inverted microscope body (Nikon UK Ltd, Surrey, UK) was used for all experiments. A range of Nikon objectives was used: 4×/0.13NA PhL, 10×/0.3NA Ph1, 20×/0.45NA Ph1 ELWD, 40×/0.6NA Ph2 ELWD, 60×/1.49NA TIRF, 100×/1.3NA (Nikon, UK). Non-phase lenses were used with a single external Ph3/60× phase ring mounted in an external phase ring turret below the trinocular head. For ultra-high-NA measurements a specialized 100×/1.65NA (Olympus) objective was used with an appropriate thread adapter, in conjunction with sapphire coverslip and index-matched immersion oil ($n = 1.78$). For SICM, 'Ionscope' ICNanoP (pipette-scanning) or ICNanoS (sample-scanning) SICM systems (Ionscope Ltd., Herts, UK) were mounted to the inverted frame with the scanned nanoelectrode parallel to the optic axis.

LED illuminator

Commercial bare LED ring printed circuit boards (PCBs: white, RGB; Ø44, 92 mm) were obtained from an online supplier (www.ebay.com) and were mounted and aligned on an adjustable retort stand using manual positioning while inspecting the objective BFP using a Bertrand lens. For the experiments in Figure 3 a new commercial instrument

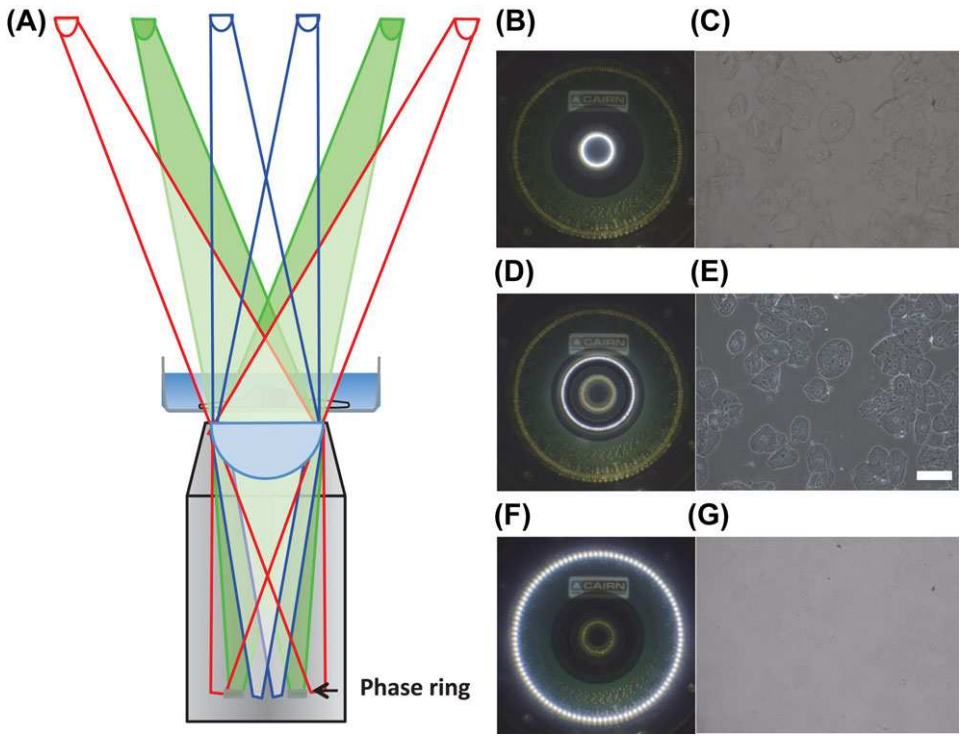

Fig. 3. Geometric matching of LED ring to phase ring suffices to produce phase contrast. (A) Schema showing three independent rings of LEDs at a fixed distance from the sample (180 mm), one of which matches the phase ring geometry *(green)*. (B) BFP image showing Ø 17 mm ring of LEDs, which appears smaller than the phase ring of the 20× 0.45NA ELWD apodised objective. (C) Corresponding field plane image to *B* showing brightfield contrast using mis-matched ring. (D) BFP image showing ring of LEDs (Ø 40 mm) matched to the phase ring. (E) Corresponding field plane image to *D*, showing excellent phase contrast (scale bar 100 μm). (F) BFP image showing Ø100 mm ring, appearing much larger than the phase ring. (G) Corresponding field plane image from *F* showing brightfield contrast using the mis-matched ring.

employing multiple concentric LED rings was employed (Aura^{TM}, Cairn Research Ltd, Faversham, UK). BFP images were acquired using a DSLR camera (Nikon D7000: Sony IMX071 16.2 megapixel CMOS sensor, pixel size 4.78 μm) attached to the eyepiece using a 2× eyepiece adapter (NDPL-1, 2× magnification, Boeco GmbH, Hamburg, Germany). Wide-field phase contrast, darkfield and Rheinberg images were acquired using a Nikon Digital Sight DS-Fi1 camera (2560 × 1920, 3.4 μm pixels, 12 bit) via a Nikon 0.6× TV lens adapter. For scanning probe experiments, bespoke LED ring PCBs were fabricated using a Ø13 mm closed ring of 24× SMD0603 emitters (Kingbright, λ_{peak} 515 nm, $\Delta\lambda_{1/2}$ 30 nm, Fig. 9D) and a Ø14 mm notched ring of 13× SMD1206 emitters (Kingbright, λ_{peak} 515 nm, $\Delta\lambda_{1/2}$ 30 nm, Fig. 9G, 10). LEDs were driven by a regulated constant-current supply and mounted inside the SICM Faraday cage using a simple bespoke positioner (Fig. 9C).

Quantitative image analysis

To quantitatively compare performance of condenserless LED phase contrast with standard commercial approaches I have adopted the method of Vainrub to obtain an approximation to the modulation transfer function (MTF) through imaging of a transmission sample containing a wide range of spatial frequencies (Vainrub, 2008). A commercial CD-ROM disc (original, not CD-RW), containing open 'pits' and closed 'lands' of the appropriate size regime (inter-track distance 1.6 μm), was imaged under identical conditions under either LED or condenser-based illumination. Images were imported into ImageJ (U. S. National Institutes of Health, Bethesda, http://imagej.nih.gov/ij/) and representative line profiles as well as Fast Fourier Transform (FFT) of 1024 × 1024 pixel subsets were extracted (Fig. 5C, D) and compared across a range of objective magnifications and numerical apertures (Fig. 5E).

Scanning ion conductance microscopy (SICM)

Cells were mounted in glass-bottomed Petri dishes inside the Faraday cage of the SICM instrument on the stage of an inverted microscope (Nikon TiEclipse). The SICM signal was referenced to a pair of AgCl electrodes, inserted into both nanoelectrode and bath. In these experiments lower-resolution images were acquired using a shutterless CMOS camera (DCM35, OpticStar, Manchester, UK) to avoid vibration. Hopping-mode

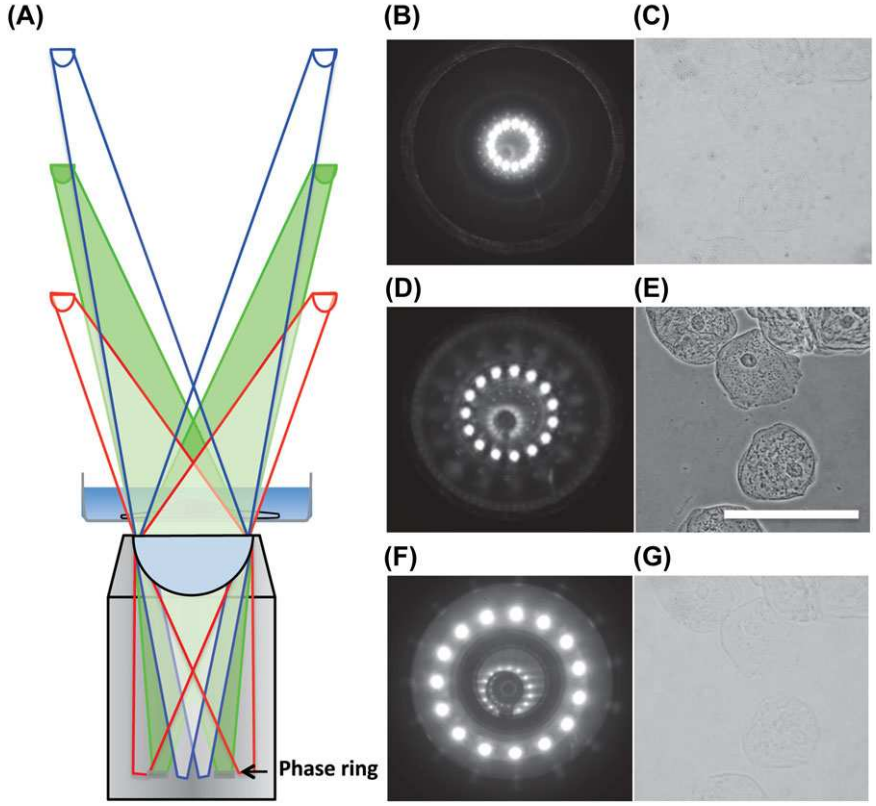

Fig. 4. Axial optimisation of LED ring diameter in the objective BFP. (A) Schema of axial adjustments to match phase ring geometry. An identical ring Ø44 mm of LEDs at three different axial positions produces images in the BFP at linearly varying diameters. At one particular position the ring overlies the phase ring of 40×/0.65NA apodised Ph2 objective (*green*), while placing the ring closer to or further away from the objective mismatches the ring to the phase ring in the objective. (B) BFP image with LED ring positioned farther than optimal (160 mm from sample), thus ring appears smaller than the phase ring in the BFP. (C) Corresponding field plane in *B*, showing low transmitted brightfield contrast. (D) BFP image showing Ø44 mm LED ring matched to phase ring diameter (at a distance of 80 mm from the sample). (I) Corresponding field plane image to *H* showing excellent phase contrast. Scale bar 100 μm. (J) BFP image showing LED ring closer than optimal (50 mm from sample), producing a ring image larger than the phase ring. (M) Corresponding field plane image to *L*.

SICM scans were obtained to show 3D morphological features of cells using either sample-scanning (ICNanoS) or pipette-scanning (IPNanoP) as described according to the experiment. 2D and 3D renderings of data sets were produced using commercial software (SPIP, Image Metrology, Hørsholm, Denmark).

Prepared slides

Fixed, clarified sample slides of butterfly head (*Vanessa Atalanta*) and hedgehog flea (*Archaeopsyllus erinacei*) were obtained, mounted in Canada balsam, courtesy of the School of Biology; Biological Photography and Imaging collection.

Results

The condenser-free phase contrast illumination schema presented here (Fig. 1B) exploits simple lens optics to ensure that a ring of LED sources placed at some distance from the sample opposite the objective lens produces an image of the emitters in the objective BFP. Inspecting the BFP of any microscope using a Bertrand lens or phase telescope provides an 'infinity' view through the objective of the area above the sample, which is very convenient for locating and centring electrodes in electrophysiology and scanning probe microscopy. It was found in this study that insertion of a ring of individual LED sources above the sample produced an image of the ring in the BFP (Fig. 1B, *inset*). Provided the distance from objective to LED ring exceeds the focal length of the objective lens, light emanating from each emitter is captured by the objective and brought into sharp focus in the BFP. Manipulation of the illuminating ring orthogonal to the optic axis produces *XY* translation of its BFP image (Fig. 2), while alteration of objective-ring distance along the optic axis produces alteration in the apparent diameter of the ring in the BFP through perspective (Fig. 4A). Multiple rings of varying diameters may be simultaneously implemented to supply phase contrast to suit various objectives which, when lit in turn, will only provide phase contrast

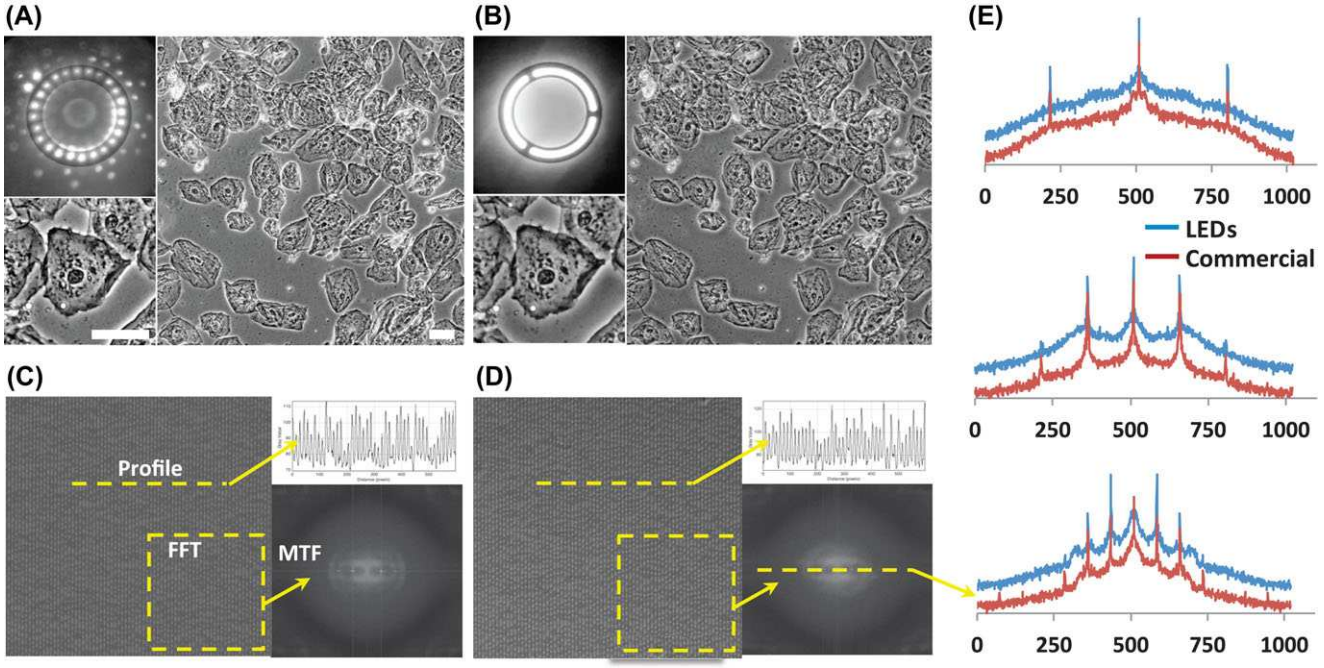

Fig. 5. (A) BFP image of conventional condenser-based annular phase contrast illumination in a 10×/0.3NA Ph1 objective. (B) Conventional phase contrast illumination (condenser NA: 0.52) of fresh buccal epithelial strew. (C) Detail (pixel subset) from image in *C*. (D) BFP image of condenser-free LED-based phase contrast illumination, showing Ø14 mm LED ring aligned with the phase ring of the same objective (sample distance 60 mm). (E) Corresponding field plane image from *D* showing excellent Zernike phase contrast using condenser-free LED ring illumination. (F) Detail from image in *E* (pixel subset). All scale bars are 50 μm.

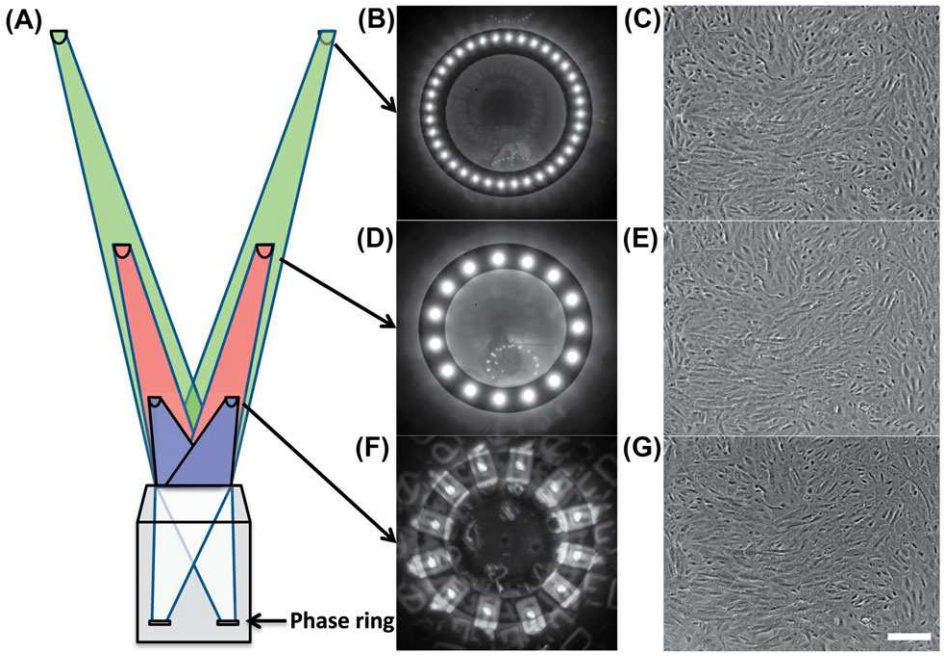

Fig. 6. (A) Geometric generalization of condenser-free phase contrast illumination using LED rings of different diameters, positioned along the optic axis such that identical geometry matches each to the objective phase ring. (B) BFP image showing Ø92 mm LED ring aligned with the phase ring of a 10×/0.3NA Ph1 objective (sample distance: 405 mm). (C) Corresponding field plane image from *B* showing excellent phase contrast in a confluent layer of ARPE-19 cells. (D) BFP image showing Ø44 mm LED ring aligned with the phase ring of the same objective (sample distance: 190 mm). (E) Corresponding field plane image from *F* in the same location as *C*. (F) BFP image showing Ø8 mm LED ring aligned with the phase ring of the same objective (sample distance: 35 mm). (G) Corresponding field plane image from *F* in the same location as *C*. Scale bar 200 μm.

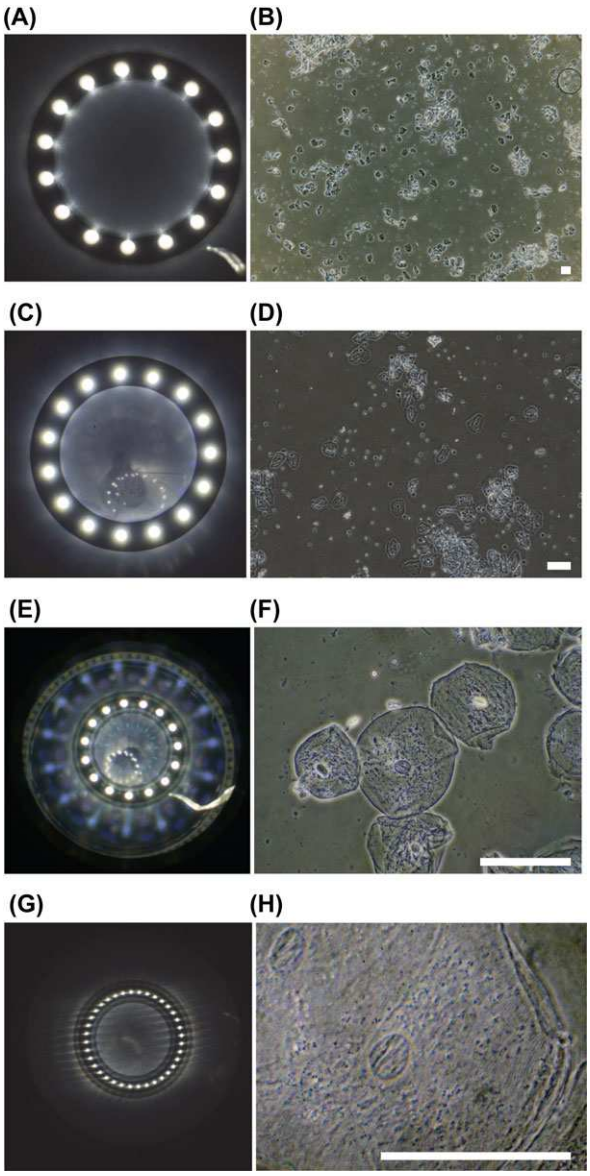

Fig. 7. Generation of condenser-free phase contrast imaging across a full range of magnifications and phase positions. (A) BFP image showing Ø44 mm LED ring aligned with the phase ring of a 4×/0.13NA PhL objective (sample distance: 455 mm). (B) Corresponding field plane image from *a* demonstrating excellent phase contrast at 4×/0.13NA PhL, scale bar 100 μm. (C) BFP image showing Ø44 mm LED ring aligned with the phase ring of a 10×/0.3NA Ph1 phase contrast objective (sample distance: 194 mm). (E) Corresponding field plane image from *D*, scale bar 100 μm. (F) BFP image showing Ø44 mm LED ring aligned with the phase ring of a 40×/0.6NA Ph2 ELWD apodised phase contrast objective (sample distance: 80 mm). (G) Corresponding field plane image from *F*, scale bar 100 μm. (I) BFP image showing Ø92 mm LED ring aligned with a Ph3 phase ring mounted in an external turret (sample distance: 15 mm), through a 100×/1.65NA objective, using a sapphire coverslip and matched immersion oil ($n = 1.78$). (E) Corresponding field plane image from *D* showing condenser-free phase contrast image at extremely high resolution, revealing detail including subtle ridging in to the cell membrane of buccal epithelia. Scale bar 50 μm.

when illumination is matched to the phase ring in the BFP (Fig. 3). In combination, the geometric flexibility conferred by this condenser-free illumination scheme allows this method to be generally applied to any conceivable range of objective magnification, numerical aperture or conventional phase position.

It was demonstrated that by progressively misaligning the LED ring with the objective phase ring, either in *XY* by translation (Fig. 2) or in *Z* by movement along the optical axis (Fig. 4) that true Zernike phase contrast is produced only when optimal alignment is maintained. In a uniform culture of confluent cells it can be seen that a zone of optimal alignment is characterized by a characteristic drop in intensity as the attenuating phase ring attentuates a portion of direct-path light (Fig. 2B). This loss in intensity is accompanied by an increase in contrast (shown in Fig. 2C as average pixel intensity ± standard deviation in each vertical column of pixels). Similarly, as the LED ring is raised or lowered, and the apparent diameter of the ring's image in the BFP is thus made smaller (Fig. 4B,C) or larger (Fig. 4F,G) than the phase ring, the phase contrast effect collapses. When correctly aligned, obtained phase contrast is excellent (Fig. 4D,E) and compares favourably with the best commercial systems available (Fig. 5). While sensitive to alignment within the BFP, the phase effect is remarkably robust to slight misalignment of the LEDs themselves, as the large optical leverage greatly diminishes the scale of any disturbing movements within the BFP. In practice, this means that alignment of the LEDs is possible using rudimentary manual positioning, and is tolerant to minor imprecisions in both alignment and tilt of the ring itself while still providing good phase contrast.

The geometric flexibility of the *XY* and *Z* adjustments detailed above allows the use of a single LED ring to produce phase contrast across different objective lenses, spanning multiple conventional phase positions (Fig. 7). Alternatively, the defined, linear, geometric relationship between distance and diameter at a single phase position allows phase contrast to be produced using LED rings of several diameters (Fig. 6), provided the requisite axial adjustments are made to match the BFP image of each ring to the phase ring inside the objective. There appears to be minimal functional distinction between the performance of LED rings from 8 to 92 mm in this particular example (Fig. 6), and rings of up to 160 mm in diameter have been successfully tested (not shown).

The phase contrast effect produced appears to be true Zernike phase contrast, created using conventional detection optics but completely abrogating the condenser assembly. Inspection of a wide field of illumination (Fig. 5A, horizontal field 866 μm at 10×) demonstrates wall-to-wall uniformity comparable to a top-flight Nikon Ti Eclipse inverted microscope using conventional condenser-based phase illumination (condenser: 0.52NA, Fig. 5B). Inspection of a representative cell as a pixel subset within these images demonstrates functional identity between the two illumination methods (*inset*, Fig. 5 A,B) suggesting that, in principle, any system could

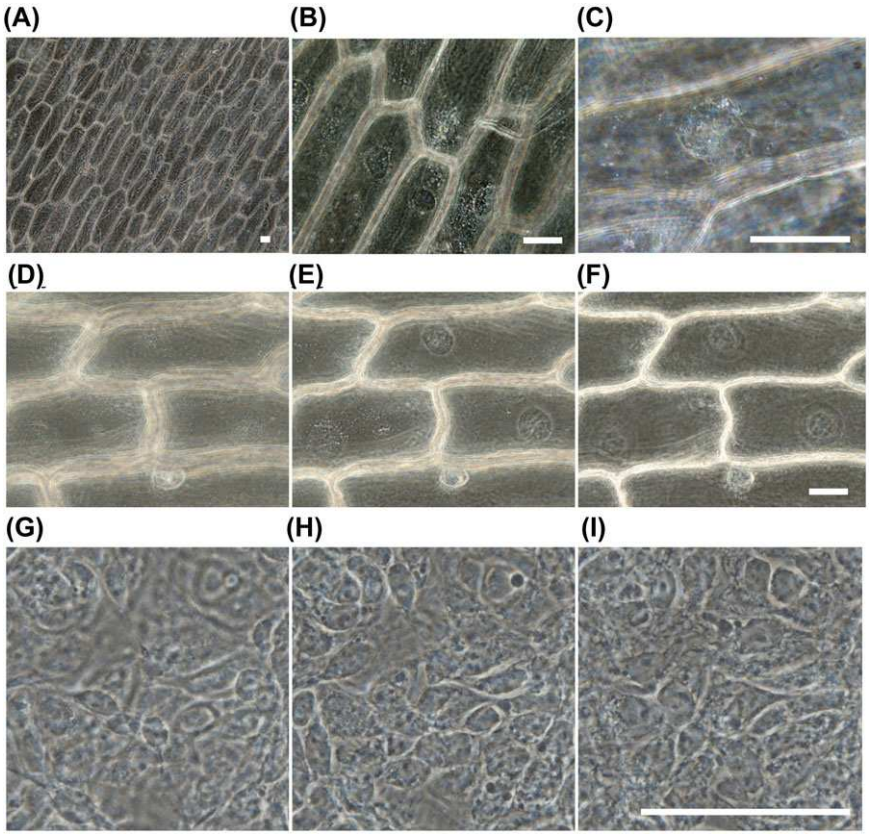

Fig. 8. Performance of condenserless phase contrast in thick samples. LED illumination (Ø44 mm) was used to perform phase contrast imaging in fresh onion skin (thickness ~100 μm) and 3D cell cultures at a range of magnifications. (A) Onion skin cells imaged at 10×/0.3NA Ph1. (B) 40×/0.6NA Ph2, (C) 100×/1.3NA Ph3. (D–F) Individual frames from a *z*-stack (1 μm/step) across a layer of onion skin at 40×/0.6NA Ph2. (D) z+20 μm reveals submembrane vesicles adjacent to the central vacuole. (E) z+60 μm reveals cell nuclei surrounded by a mobile vesicle population (see Supplementary videos for dynamic time-lapse imaging). (F) z + 100 μm reveals a further submembrane vesicle population on the other side of the vacuole (all scale bars 50 μm). **(G–I)** Phase contrast imaging in a 3D culture of human rhabdomyosarcoma cells, revealing multiple overlying cell layers. (G) Upper layer of transdifferentiated cells lies on top of the culture (z = 0 μm). (H) Deeper layer of cells and top of 'feeder' layer revealed at z+10 μm. (I) Nuclei and lower attachments of 'feeder' layer are revealed at z+20 μm (scale bar 50 μm). See Supplementary materials for dynamic video of through-focussing within this stack of images.

benefit from use of this illumination schema with no compromise in performance. To provide a quantitative comparison the method of Vainrub was applied (Vainrub, 2008) to extract an approximation to the system modulation transfer function (MTF) using various objective lenses (Fig. 5D,E). Using a sample comprising a wide range of spatial frequencies this FFT-based approach reveals a close match between condenserless LED phase illumination versus commercial condenser-mediated phase contrast (Fig. 5E). In summary the method would appear to deliver both functionally as well as quantitatively equivalent images to the best commercial systems.

To evaluate the geometric generalizibility of the condenser-free phase contrast illumination schema a wide range of objective lens magnifications and numerical apertures was tested using a single fresh buccal epithelial sample (Fig. 7). Excellent phase contrast was obtained at each of 4×/0.13NA PhL (Fig. 7A,B), 10×/0.3NA Ph1 (Fig. 7C,D), 40×/0.6NA Ph2 (Fig. 7E,F), and 100×/1.65NA Ph3 (Fig. 7G,H). The success obtained using such a wide range of magnifications (4–100×), numerical apertures (0.13–1.65) and phase positions (PhL-Ph3) strongly implies that the condenser-free phase contrast schema is completely generalizable to cope with the full range of optical microscope objectives in general use. Normally very high NA objective lenses require correspondingly high-NA condenser assemblies to achieve phase contrast, which are both expensive and very restrictive in terms of space above the sample. The same schema has been demonstrated successfully using a TIRF lens 60×/1.49NA (Fig. 11) as well as a specialized ultrahigh-NA objective lens (100×/1.65NA Olympus) using a sapphire coverslip and high-index immersion oil (n = 1.78). Excellent phase contrast to the subtle membrane and subcellular features was obtained in buccal epithelia using these demanding objectives (Fig. 7G,H) in combination with an external phase ring (Ph3). Buccal epithelia, while

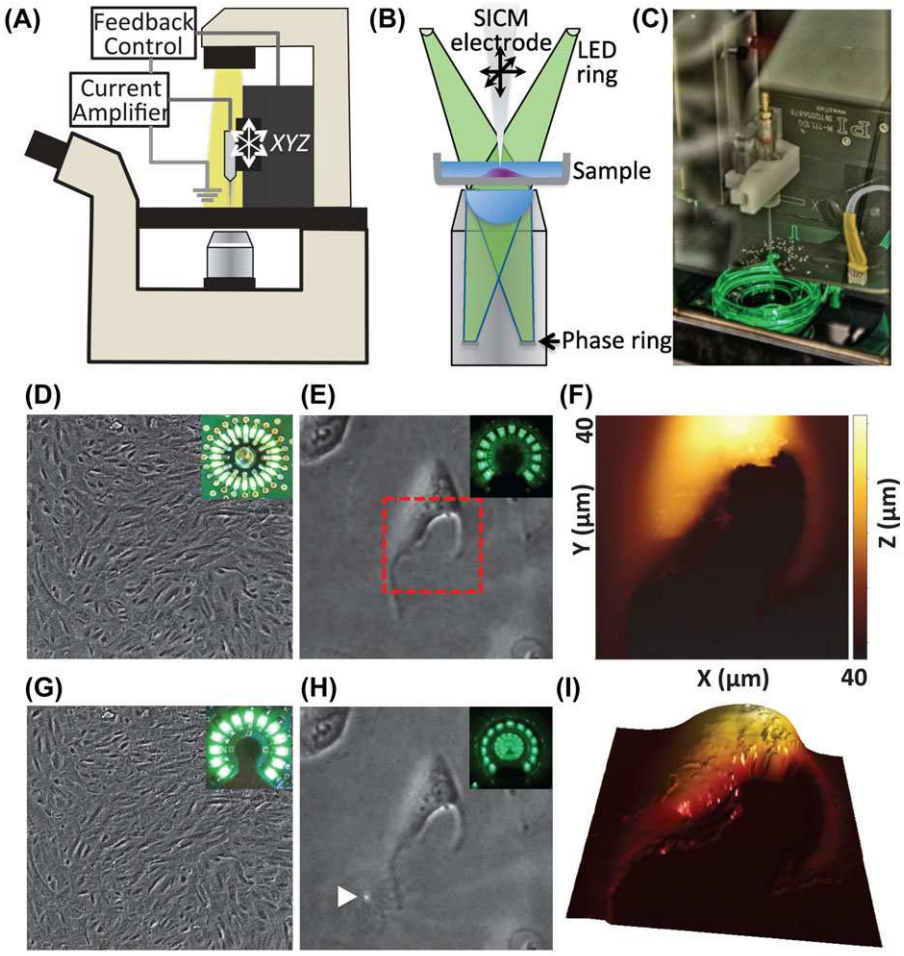

Fig. 9. (A) Scanning ion conductance microscopy on an inverted microscope. A glass nanoelectrode is moved under closed-loop feedback referenced to current leaving the tip, and is scanned in *XYZ* to build an image. The electrode holder and motion control apparatus preclude a condenser assembly. (B) Illumination schema for condenser-free phase contrast under SICM such that a ring of LEDs, (1206 SMD, 13 emitters, Ø14 mm), notched to admit a scanning probe, surrounds the electrode. (C) LED illuminator PCB in working position around the electrode of the SICM instrument (ICNanoS, Ionscope Inc, Herts, UK). (D) Confluent ARPE-19 cells imaged in phase contrast at 10×/0.3NA Ph1 using a closed LED ring (0603 SMD, 24 emitters, Ø13 mm *(inset)*, sample distance: 57 mm). (E) ARPE-19 cell under condenser-free phase contrast illumination (40×/0.6NA ELWD Ph2) using a notched ring (1206 green SMD, 13 emitters, Ø14 mm *(BFP inset)*, sample distance: 25 mm, scale box 40 μm). (F) SICM image, using sample-scanning in hopping mode. (G) Same cell area as *d* imaged using a notched LED ring. (H) ARPE-19 cell under condenser-free phase contrast observation as in *D*, but with electrode inserted (Δ), phase contrast imaging is not compromised *(BFP Inset)*. (i) 3D rendering of dataset in *F*. Reproduced with permission from Webb *et al.* (2013).

excellent test subjects for phase contrast imaging in general, are axially rather thin samples. To verify performance of the condenserless LED schema in thick samples, images were obtained from the very thick (100 μm) cell layers of fresh onion skin (Fig. 8A–F). Confluent cultures of human rhabdomyosarcoma cell line TE671, which spontaneously forms multilayered cultures *in vitro* (Fig. 8G–I), were also imaged. See also Supplementary material for dynamic images from these preparations.

In a parallel series of experiments, the effect of missing LED sources within the ring was tested with the aim of creating a 'notch' to fit the illuminator around the electrode of a SICM which, due to its construction and mounting to the inverted microscope frame, precludes the use of a phase contrast condenser assembly (Fig. 9A). Two similarly sized bespoke PCBs were fabricated and each tested against the performance of a commercial phase contrast microscope. The performance of a fully closed ring (Fig. 9D) appeared functionally indistinguishable from the commercial condenser, while the omission of emitters covering ~30° of the ring also produced functionally equivalent images (Fig. 9G), suggesting that the incorporation of the notch does not appreciably degrade imaging performance while admitting a scanned probe for simultaneous multimodal imaging.

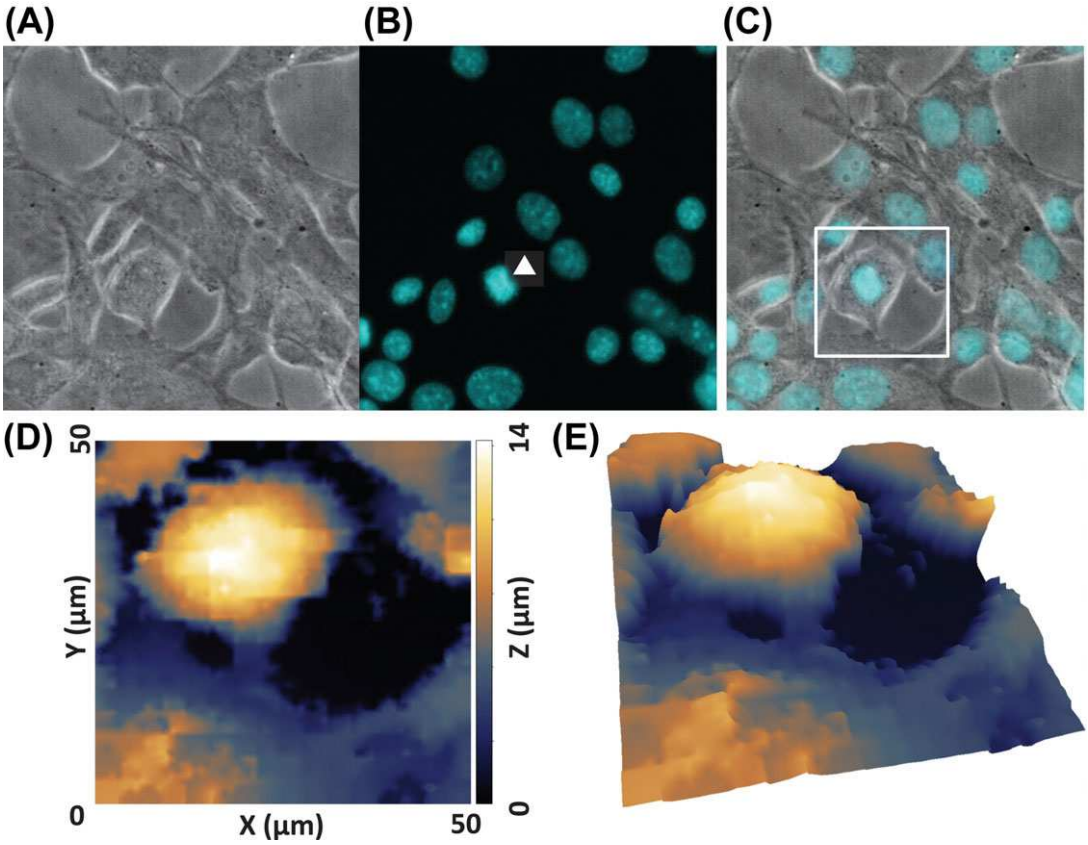

Fig. 10. Multimodal imaging using concurrent condenser-free phase contrast, scanning ion conductance microscopy and epifluorescence. (A) 3T3 fibroblasts under condenser-free phase contrast illumination (60×/1.49NA Ph3). Scale box 50 μm. (B) 3T3 cells from *a*, DNA stained with Hoechst. Cells with condensed chromatin, as inside the box, are about to divide (Δ). (C) Overlay of panels *A,B* showing target cell in prophase. (D) Hopping-mode pipette-scanning SICM image (ICNanoP, Ionscope Inc., Herts, UK) of boxed cell in panels *A*–*C*. (E) 3D rendering of dataset in *D*. Reproduced with permission from Webb *et al.* (2013).

On the basis of this finding, a series of experiments was performed using both sample-scanning (ICNanoS, Fig. 9) and probe-scanning (ICNanoP, Fig. 10) SICM systems (Ionscope Ltd). The bespoke PCBs were mounted by a miniature positioning system to fit around the scanning electrode (Fig. 9B) and the entire assembly fitted inside the Faraday cage built around the SICM system (Fig. 9C). It was found that not only was excellent phase contrast obtained when the LEDs were appropriately aligned with the phase ring (Fig. 9E) but also that inserting the electrode and bringing it into working position with the sample did not appreciably compromise the imaging performance (Fig. 9H). Combined multimodal imaging was demonstrated by performing hopping-mode scans of ARPE-19 cells (Fig. 9F), using sample scanning to produce rendered images of 3D cell morphology (Fig. 9I). To test whether moving the electrode in the *XY* plane was deleterious to phase contrast imaging further experiments were performed using hopping-mode pipette scanning (Fig. 10). Expanding cultures of 3T3 fibroblast cells were fixed to freeze cytokinesis, and DNA was labelled with Hoechst stain to reveal cells in the process of dividing (Fig. 10B). Multimodal images (parallel SICM, epifluorescence, Zernike phase contrast) were obtained from individual dividing cells using a TIRF lens (Fig. 10A–C) and rendered to reconstruct cell morphology (Fig. 10D,E) with excellent observability throughout in both phase contrast and epifluorescence at 60×/1.49NA. This combination of condenser-free Zernike phase contrast and SICM imaging has been briefly reported elsewhere (Webb *et al.*, 2013).

Darkfield and Rheinberg illumination

As a natural extension to the condenser-free phase illumination schema outlined above, the possibility of condenser-free darkfield illumination was explored using LED rings. Lowering the LED ring below the phase contrast position resulted in progressively increasing diameter of its BFP image until the LED emitters moved 'outside' the BFP (Fig. 11A). A comparison schema is shown in Figure 11(B), showing how light entering the objective occupies such an extreme angle that it doesn't transit the objective, losing itself into the darkened wall of the

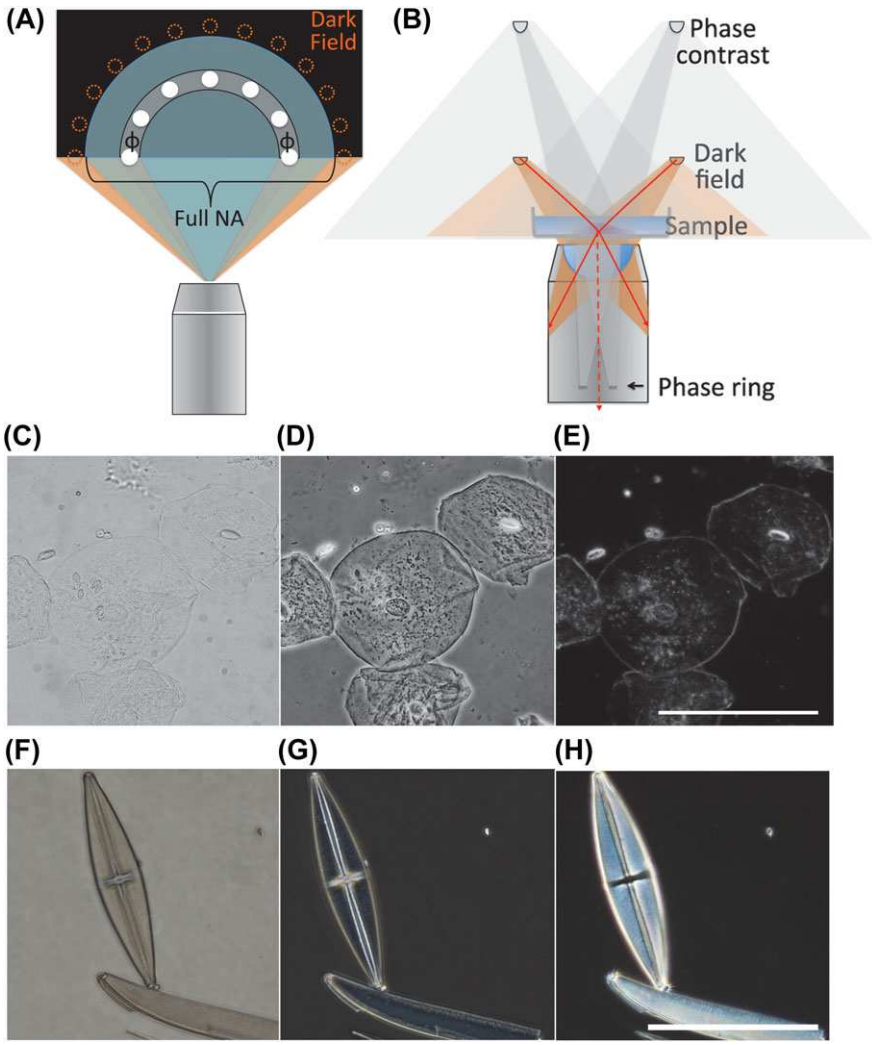

Fig. 11. Exploiting condenser-free geometric adjustment to yield both phase contrast and darkfield contrast in a preparation of fresh buccal epithelial cells by shifting the axial position of the LED ring. (A) Back focal plane schema for phase contrast and darkfield illumination, showing the relative positioning of LED ring for phase contrast (Φ) and darkfield illumination (dashed circles), where the ring is lowered such that LEDs are not visible on inspecting the BFP. (B) Illumination schema for phase contrast (white) and darkfield illumination (orange) using a single ring of LEDs. Light scattered by the sample enters the optical path (dashed lines) to create condenser-free darkfield contrast. (C) Brightfield image at 40×/0.6NA demonstrating low transmitted-light contrast in buccal epithelia. (D) Condenser-free phase contrast image at 40×/0.6NA Ph2 from the same location as *C*. (E) Darkfield image of same field in *C,D* showing excellent condenser-free darkfield contrast (scale bar 100 μm). (fF) Brightfield image at 40×/0.6NA demonstrating low transmitted-light contrast in a diatom strew. (G) Condenser-free phase contrast image at 40×/0.6NA Ph2 from the same location as *F*. (H) Darkfield image of same field in *F, G* showing excellent condenser-free darkfield contrast (scale bar 100 μm).

objective tube (*solid lines* Fig. 11B). In the absence of a sample, a pure black field is seen; when a sample is introduced light scatter from small features and discontinuities results in light entering the objective lightpath (*dashed lines*, Fig. 11B). Buccal epithelial (Fig. 11C–E) and diatom strews (Fig. 11F–H) were examined using condenserless brightfield, phase contrast and darkfield. Tiny vesicular bodies, edge discontinuities and other subcellular features of the cells were easily visualized, with excellent contrast against a pure black field. In the absence of the sample, the dark field was completely blank (not shown).

In addition to darkfield, it was interesting to exploit this condenser-free schema to implement combinatorial techniques such as Rheinberg illumination, where colour contrast is obtained by combining coloured transmitted illumination with darkfield illumination in a contrasting colour (Fig. 12B). Using a single diffused central cyan LED as brightfield illumination source, along with a ring of orange LEDs in darkfield configuration (Fig. 12A), it was possible to obtain sequential condenser-free darkfield and brightfield images *(inset)*. Using both LED sources in parallel resulted in single-shot Rheinberg illumination images (Fig. 12B,C) which could be adjusted

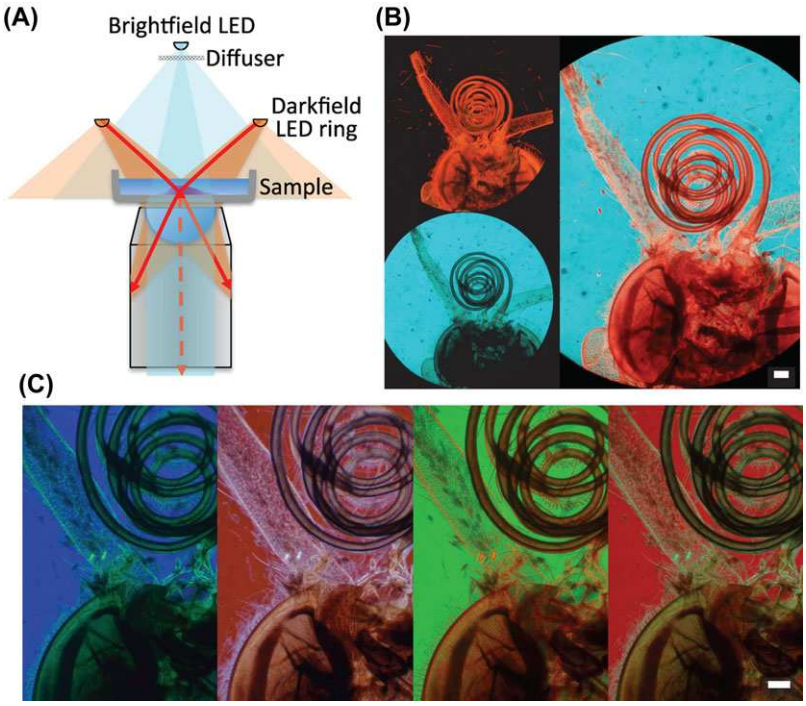

Fig. 12. Condenser-free Rheinberg illumination. (A) Schema of LED-based condenser-free Rheinberg illumination, using a single central diffused LED for transmitted brightfield imaging (*cyan*) in parallel with a contrasting ring of LEDs in the darkfield position (*orange*). (B) Condenser-free Rheinberg image of a butterfly head (*Vanessa atalanta)* taken using orange LED ring in darkfield and cyan in brightfield *(inset)*. (C) Flexibility in colour contrast conferred by using RGB LEDs in both brightfield and darkfield positions in *b* at 4×/0.13NA (scale bar 200 μm).

arbitrarily to match varying objectives. To further demonstrate the potential of the method RGB LEDs were used in each of the central and ring positions, allowing independent adjustment of the colours in both brightfield and darkfield to produce arbitrary Rheinberg colour contrast (Fig. 12C).

As a final demonstration of simultaneous multimodal condenser-free contrast for transmitted-light microscopy a system was constructed using two LED rings and a single central LED, allowing the satisfaction of brightfield, darkfield and phase contrast according to the illustration (Fig. 13B) and geometric schema shown in Figure 13(A). By illuminating each ring in turn, high quality images were produced in sequence of phase contrast (Fig. 13C), darkfield (Fig. 13C) and Rheinberg illumination (Fig. 13G). Turning on all three LED sources together produced an image unlike any of the others alone (Fig. 13E). This image represents the simultaneous evocation of brightfield, darkfield and phase contrast in a multimodal regime whose potential may be considerable in challenging samples, since the spectral content and relative intensity of each component may be arbitrarily and flexibly manipulated. Textural and morphological detail is thus considerably enhanced, yielding tunable, visually compelling contrast.

Discussion

Phase contrast microscopes have become ubiquitous workhorses in the biomedical research lab, from basic cell culture observation systems to advanced research microscopes. While the technique is not expensive, in comparison with advanced methods such as differential interference contrast (DIC), it requires multiple optical and mechanical components to achieve the requisite Köhler conjugation of planes and alignment of the phase annulus with the phase ring. The key observation of the current work is that so long as the image of a ring of LED emitters appears in the BFP of the objective, conjugate and aligned correctly with the phase ring, the result is true Zernike phase contrast. Excellent contrast is obtained despite the absence of a field diaphragm, even in thick samples where multiple layers of cells are resolvable within 3D cell cultures (Fig. 8G–I) and subcellular dynamics are visualizable even in 100 μm thick onion cells at a range of magnifications up to 100×, 1.3NA (Fig. 8A–F, see also Supplementary materials). The condenser-free schema, using the objective itself to project the LED emitters into the BFP, can be flexibly adapted using simple geometry to a range of objective magnifications and conventional phase positions.

The method has been tested with phase contrast objectives from all four major manufacturers of commercial systems, and has been found to work equally well for each provided attention is paid to proper alignment by observing the BFP. A major advantage of the method, along with its relative simplicity of design, alignment and flexibility between objective lenses, lies in the significantly enhanced working distances

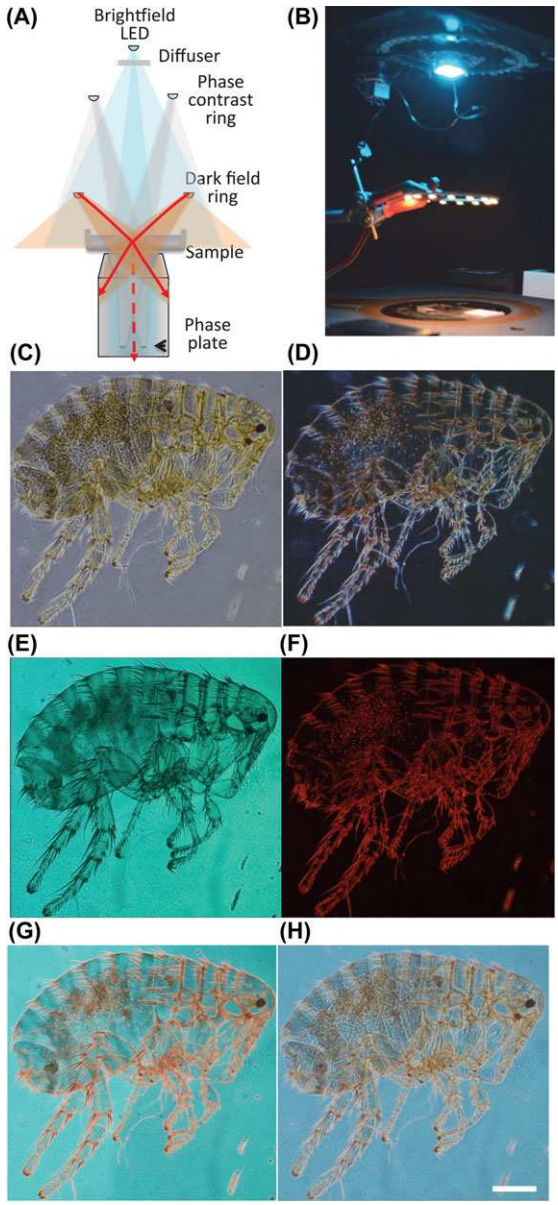

Fig. 13. Multimodal condenser-free imaging conferred by LED illumination schema. (A) Schema showing the implementation of parallel brightfield, phase contrast and darkfield imaging using condenser-free LED illumination. Matching the appropriate geometry allows either sequential or simultaneous imaging using separate transmitted brightfield (*cyan*), phase contrast (*white*) and darkfield (*orange*) illumination. (B) Combinatorial condenserless illumination system in use for Rheinberg illumination. Note the simple positioning retort, and extended working distance. (C) Condenser-free phase contrast image of hedgehog flea (*Archaeopsyllus erinacei)* at 4×/0.13NA. (D) Condenserless darkfield image (using white LEDs) of sample in (*C*). (E) Brightfield image obtained of sample in *c* using central diffused cyan LED. (F) Orange LED in darkfield configuration obtained from sample in *C*. (G) Rheinberg illumination created by simultaneous illumination with brightfield (*cyan*) and darkfield (*orange*) LEDs. (H) Simultaneous phase contrast, transmitted brightfield and darkfield illumination of sample in (*C*), using all three LED systems simultaneously (scale bar 500 μm).

possible between the illumination assembly and the sample. For comparison, images in Figures 6 (B) and (C) were acquired using a Ø92 mm ring with a sample distance of 180 mm; acquiring a comparable image using standard commercial phase condenser would provide a working distance of less than 50 mm.

The condenser-free phase contrast illumination scheme elaborated in this paper (Fig. 1B) is fully compatible with existing phase contrast optics, including apodised objectives, as well as being potentially generalizable to random-source, quantitative phase stepping and other allied phase methods. It will be interesting in future papers to investigate whether a similar approach, but lighting only one or several emitters at a time, could further satisfy the requirements for the aperture-scanning phase contrast microscope embodied by Ellis using a vibrating optical fibre and moving phase ring (Ellis, 1988). Replacing the scanned components with a fixed ring of independent emitters lit in concert with a spatial light modulator may provide such a system free of moving parts. Similarly, the advanced diffraction tomography recently implemented using lasers scanned via the condenser assembly (Fiolka *et al.*, 2009) and the full-NA, randomized phase contrast embodied by Maurer may be tractable using this simplified, condenser-free approach (Maurer *et al.*, 2008).

In addition to visible light, there would seem to be no barrier to obtaining condenser-free phase contrast in other regions of the electromagnetic spectrum employing either aperture scanning or arrays of independent emitters of X-rays, UV or the infrared. The simplified optical design may make possible both phase and darkfield contrast in these exotic wavebands without the need for diffractive or other elaborate condenser optics (Neuhausler & Schneider, 2006). Condenser-free imaging should thus reduce the complexity and cost of such systems in future, as well as provide for flexibility in geometric adjustment – a nontrivial goal to achieve in these regimes (Kimura *et al.*, 2013).

It is possible that the chosen cell samples inherently mask any small artefacts induced by omission of emitters or, by analogy, of the discretization of the ring into multiple independent sources. Analysis of any such effects awaits a full theoretical treatment of the schema. The current work convincingly argues for functional equivalence in the hands of the researcher pursuing multimodal imaging with scanning probes, addressing cells with electrodes, or requiring additional access to the preparation.

Interestingly, it was not found necessary for condenser-free phase contrast to angle the emitters of the LEDs towards the objective lens, even at very high NA, due to the wide pseudo-Lambertian emission of 'white' phosphor-coated LEDs. No attempt was made to vary the angle of LED emission in the experiments presented. Directing the centre of each emitter towards the objective was found to increase the amount of light entering the imaging system, as expected from their emission profile imposed by the phosphor coating (emission angle 120°,

not shown), at the cost of more complex fabrication. Some experiments employing bespoke PCB's (Fig. 9, 10) used single-wavelength LEDs fitted with individual 'collimating' lenses (emission angle 60°), which did not detrimentally affect performance and resulted in greater light throughput due to the larger fractional solid angle captured. The apparent size of the LED emitters in the BFP is commensurately diminished by increasing the distance from the sample, as predicted by perspective. This does not appreciably decrease image quality, however it is noted that the captured light intensity is diminished with distance due to a diminution of solid angle entering the objective. Modern, intense LED sources largely negate this issue by providing sufficient light flux, the uncaptured fraction of which further provides a useful work light in and around the preparation.

Using the equipment available it was not possible to obtain darkfield at higher magnifications than 40×, since the angular requirements of annular darkfield in objectives of NA > 1 could not be met due to refraction from the upper coverslip. The surface meniscus prevented correct alignment when this coverslip was omitted. Condenser-free darkfield illumination in very high-NA objectives may be possible in future using an immersed ring illuminator without requiring expensive and rare mirror-based darkfield condenser equipment. Interestingly it was possible to satisfy the phase contrast regime of a specialized Olympus objective lens (100×/1.65NA) on a Nikon microscope body, despite the differences in tube lens length, provided the external phase ring was made conjugate with the image of the LEDs. This ability to match phase illumination to arbitrary specialized or antiquated equipment is a particular strength of the method, and may allow resurrection or hybridization of dormant equipment, repurposing within bespoke assemblies or the refurbishment and robustification of microscopes for deployment in the developing world.

The integration of several allied contrast methods into a single instrument composed of one or more rings complemented with central LED illumination further promises to allow multimodal or combinatorial imaging, several configurations of which have been recently demonstrated but requisite illumination system using conventional imaging is highly specialized and complex (Piper & Piper, 2012a, 2012b, 2012c, 2013a, 2013b). Using the simple system detailed here, the intensity and spectral composition of each illuminating component is easily and arbitrarily variable to bring out the best in particular samples. Potential embodiments using individual LEDs or short segments of the ring would provide analogous illumination to so-called 'relief contrast', useful to improve contrast in thick samples (Piper, 2007). By sequentially moving these individual or grouped sources around the ring, with complementary scanning phase element, it may be possible to achieve aperture scanning in the manner of Ellis (Ellis, 1988) while eliminating several degrees of complexity. It should also be noted that polarization of each individual emitter may allow a very simple radially polarized beam to be generated, which may be of use in highlighting birefringent structures within certain samples (Oldenbourg, 1996).

Conclusion

Condenser-free transmitted-light contrast enhancement by Zernike phase contrast and darkfield microscopy has been demonstrated using simple rings of LED sources. It is to be hoped that application of this approach will result in highly efficient and convenient illuminators for microscopy. It seems clear that this condenser-free illumination schema is general in nature. In principle the approach can be applied to any sample to which conventional phase contrast illumination is amenable; including either upright, inverted, bespoke or multimodal imaging systems. The principal advantages are the flexibility of geometric adjustment, conferring either large working distances between illuminator and stage as well as the ability to miniaturize the illumination system for highly compact microscopes of the future. Phase contrast microscopes will be greatly simplified in terms of alignment, while also providing for large working distances and arbitrary illumination spectra. Geometric flexibility will also allow matching of phase contrast or darkfield illumination to any particular objective lens or phase position, even if complementary equipment is no longer available or not supported by any particular microscope. In addition, there is little complexity or cost burden associated with implementing multiple illuminating structures in parallel. These may be sequentially or simultaneously lit to provide phase contrast, darkfield, brightfield, or any combination thereof. In principle the method is potentially applicable at any waveband across the electromagnetic spectrum. Condenser-free contrast enhancement using multiple independent illumination sources thus has the potential to increase the scope for biological imaging in labs without access to large amounts of funding or equipment.

Acknowledgements

This work was supported by a Royal Academy of Engineering/EPSRC Postdoctoral Fellowship. The author wishes to thank Prof. W.B. Amos and Prof. M.G. Somekh for critical reading of the manuscript and Dr. F.C. Pascut for excellent discussions. Thanks to Dr. N.S. Johnston for bespoke printed circuit boards, to Dr. Emilia Moradi for preparing cell cultures and to Dr. Thomas Hartman for prepared slides.

References

Ellis, G.W. (1988) An annular scan phase-contrast scanned aperture microscope (ASPSAM). *Cell Motil. Cytoskeleton* **10**, 342.

Fiolka, R., Wicker, K., Heintzmann, R. & Stemmer, A. (2009) Simplified approach to diffraction tomography in optical microscopy. *Opt. Exp.* **17**, 12407–12417.

Kempson, D.A. (1950) Low-power phase-contrast microscopy without a condenser. *Quart. J. Microsc. Sci.*, **s3–91**, 109–110.

Kimura, T., Matsuyama, S., Yamauchi, K. & Nishino, Y. (2013) Coherent x-ray zoom condenser lens for diffractive and scanning microscopy. *Opt. Express* **21**, 9267–9276.

Lugmaier, R. A., Hugel, T., Benoit, M. & Gaub, H. E. (2005) Phase contrast and DIC illumination for AFM hybrids. *Ultramicroscopy* **104**, 255–260.

Maurer, C., Jesacher, A., Bernet, S. & Ritsch-Marte, M. (2008) Phase contrast microscopy with full numerical aperture illumination. *Opt. Express* **16**, 19821–19829.

Neuhausler, U. & Schneider, G. (2006) Non-destructive high-resolution X-ray imaging of ULSI micro-electronics using keV X-ray microscopy in Zernike phase contrast. *Microelectr. Eng.* **83**, 1043–1046.

Oldenbourg, R. (1996) A new view on polarization microscopy. *Nature* **381**, 811–812.

Otaki, T. (2000) Artifact halo reduction in phase contrast microscopy using apodization. *Opt. Rev.* **7**, 119–122.

Piper, J. (2007) Relief-phase-contrast – a new technique for phase-contrast light microscopy. *Microsc. Anal.* **21**(4), 9–12.

Piper, T. & Piper, J. (2012a) Axial phase-darkfield-contrast (APDC), a new technique for variable optical contrasting in light microscopy. *J. Microsc.* **247**, 259–268.

Piper, T. & Piper, J. (2012b) Variable Phase-darkfield Contrast (VPDC) – a variant illumination technique for improved visualizations of transparent specimens. *Microsc. Microanal.* **18**, 343–352.

Piper, T. & Piper, J. (2012c) Variable bright-darkfield-contrast, a new illumination technique for improved visualizations of complex structured transparent specimens. *Microsc. Res. Tech.* **75**, 537–554.

Piper, T. & Piper, J. (2013a) Universal variable brightfield-darkfield contrast: a variant technique for improved imaging of problematic specimens in light microscopy. *Microsc. Microanal.* **19**, 1092–1105.

Piper, T. & Piper, J. (2013b) Variable phase bright-field contrast (VPBC) – an attractive illumination technique for improved imaging in transparent specimens. *Microsc. Microanal.* **19**, 11–21

Rheinberg, J. (1896) On an addition to the methods of microscopical research, by a new way optically producing colour-contrast between an object and its background, or between definite parts of the object itself. *J. R. Microsc. Soc.* **16**, 373–388.

Vainrub, A. (2008). Precise measurement of the resolution in light microscopy using Fourier transform. *Rev. Sci. Instrum.* **79**: 046112–1 to 046112–3.

Webb, K. F., de Fillipi, G. & Johnston, N. A. (2013) Condenser-free zernike phase contrast imaging for scanning probe microscopy. *Microsc. Anal.* **27**, 27–32.

Zernike, F. (1942a) Phase contrast, a new method for the microscopic observation of transparent objects. *Physica* **9**, 686–698.

Zernike, F. (1942b) Phase contrast, a new method for the microscopic observation of transparent objects part II. *Physica* **9**, 974–986.

Zernike, F. (1953) Nobel lecture: How I discovered phase contrast. *Nobel Prize in Physics*. Elsevier Publishing Company, Amsterdam.

Supporting Information

Additional Supporting information may be found in the online version of this article at the publisher's website:

"*Onion skin z stack, 40×, 1 μm steps, 110 μm thick.mp4*". Shows an axial (z) focal series at 40μ/0.6NA Ph2, 1 μm per step, of 110 μm total thickness. The dynamics of submembrane vesicular pools is visualized throughout the full axial scan in excellent phase contrast.

"*Onion skin subcellular dynamics, 100×, timelapse 5 s image.mp4*". Shows a dynamic picture of vesicular streaming around the nucleus within a single onion skin cell at 100×/1.3NA Ph3, 5s/image. Excellent phase contrast is obtained at the plane of focus, with a clear view of subcellular dynamics at an imaging depth of 20 μm inside the sample.

"*Rhabdomyosarcoma cells, 60× z stack 0.5 μm steps.mp4*". Shows an axial (z) focal series through a multi-layered 3D cell culture of human rhabdomyosarcoma cells *(TE671)* at 60×/1.4NA Ph3, at 0.5 μm/step. A clear view is obtained throughout the culture (total thickness 40 μm), showing clearly the populations of cells which overlie layers beneath.